Arch. Mech., **59**, 4–5, pp. 365–384, Warszawa 2007

Effect of aggregate structure on fracture process in concrete using 2D lattice model

J. KOZICKI, J. TEJCHMAN

Faculty of Civil and Environmental Engineering
Gdańsk University of Technology
80-952 Gdańsk-Wrzeszcz, ul. Narutowicza 11/12

THE 2D LATTICE MODEL was used to analyse fracture processes in concrete at the meso–level. Concrete was described as a three–phase material (aggregate, interfacial transition zone and cement matrix). The calculations were carried out for concrete specimens subject mainly to uniaxial extension. The effect of the aggregate density was investigated. In addition, a deterministic size effect was studied. The advantages and disadvantages of the model were outlined.

Key words: concrete, fracture process, 2D lattice model, aggregate density

1. Introduction

FRACTURE PROCESS is a fundamental phenomenon in brittle materials [3]. It is a major reason of damage in brittle materials under mechanical loading, contributing to a significant degradation of the material strength. It is highly complex due to a heterogeneous structure of brittle materials over many different length scales, changing e.g. in concrete from a few nanometers (hydrated cement) to the millimeters (aggregate particles). Therefore, the material heterogeneity should be taken into account when modelling the material behavior. At the meso–level, concrete can be considered as a three–phase material consisting of aggregate, cement matrix and interfacial transition zone (bond). A realistic description of the fracture process is of major importance to ensure safety of the structure and to optimize the behavior of material.

The phenomenon of propagation of the fracture process in brittle materials can be modelled with continuous and discrete models. Continuum models describing the mechanical behavior of concrete were formulated within, among others, nonlinear elasticity [24, 29, 33], rate-independent plasticity [9, 23, 30, 31, 37], damage theory [10, 17, 19, 36], endochronic theory [4, 7], coupled damage and plasticity [16, 22, 23] and microplane theory [6]. To model the thickness and spacing of strain localization properly, continuum models require an extension in the form of a characteristic length. Such an extension can by done with strain gra-

dient [13, 32, 34–36, 51], viscous [41, 42] and non-local terms [2, 5, 8, 38]. Other numerical technique which also enables to remedy the drawbacks of a standard FE-method and to obtain mesh-independent results during the description of the formation of strain localization, is a strong discontinuity approach allowing for a finite element with a displacement discontinuity [1, 40, 50].

Within discrete methods, the most popular ones are: classical particle DEM [15, 18], interface element [12] and lattice methods [21, 28, 39, 44, 48, 49].

The lattice models are the simplest discrete models to simulate the development and propagation of fracture in brittle materials consisting of a main crack with various branches, secondary cracks and microcracks. They allow a straightforward implementation of the material heterogeneity which is projected on a lattice and the corresponding properties are assigned to relevant lattice elements.

The intention of the paper is to describe and to understand the mechanism of fracture in concrete specimens during uniaxial extension. The own 2D lattice model was used. In contrast to other lattice models [28, 39, 44, 48], a geometric type lattice model was used what is a novelty. The calculations were performed with concrete considered as a three-phase material (aggregate, cement matrix and interfacial transition zone). Attention was paid to the effect of the aggregate density (ratio between the number of aggregate elements and total number of elements) on the material behavior. For comparison, the numerical experiments were also carried out with concrete specimens described (for the sake of simplicity) as a one- and two-phase material (aggregate and cement matrix). In addition, the deterministic (energetic) size effect was analyzed with two notched specimens of different dimensions. The numerical results were compared with those obtained with a conventional lattice model [28, 39, 44, 48].

2. Model

In the case of lattice models, one can distinguish two quite different types. In the first type model (used to describe the fracture process in concrete or reinforced concrete [48, 44, 39, 28]), each quasi-brittle material is discretized as a network of two-noded Bernoulli beams that transfer normal forces, shear forces and bending moments. Fracture is simulated by performing a linear elastic analysis up to failure under loading and removing a beam element that exceeds the tensile strength. Normal forces, shear forces and moments are calculated using a conventional simple beam theory. A special factor α is used for varying the amount of bending. When it decreases, the compressive behavior changes from brittle to a ductile one. The stiffness matrix is constructed for the entire lattice. The displacement vector is calculated similarly as in the conventional FEM (by multiplication of the inverse global stiffness matrix with the load vector). The heterogeneity of the material is taken into account by assigning different

MOST WIEDZY Downloaded from mostwiedzy.pl

strengths to beams (using a Gaussian or Weibull distribution) or by assuming random dimensions of beams and random geometry of the lattice mesh, or by mapping of different material properties to beams corresponding to the cement matrix, aggregate and interfacial transition zone (Fig. 1) in the case of concrete. To obtain aggregate overlay in the lattice, a Fuller curve is usually chosen for the distribution of grains. The ratio between the beam height and the beam length determines the Poisson's ratio. The beam length in concrete should be less than $l_b < d_a^{\min}/3$ (where $d_a^{\min}$ is the minimum aggregate diameter).

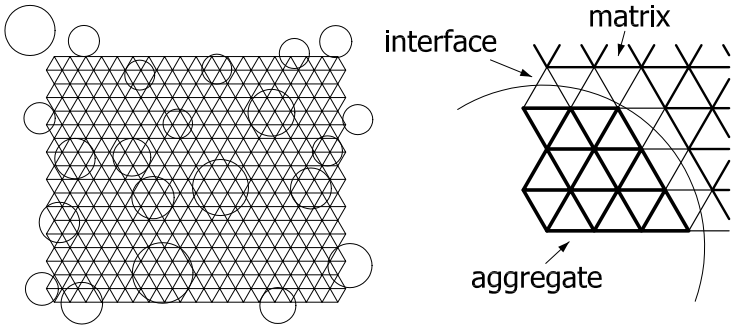

FIG. 1. Lattice of beams for concrete consisting of aggregate, cement matrix and interface [44].

The model can identify micro-cracking, crack branching, crack tortuosity and bridging which lead to the fracture process, to be followed until complete failure [44, 49]. It enables also to capture a deterministic size effect during tension [46, 49].

The advantages of this approach are simplicity and a direct insight in the fracture process on the level of the micro-structure. A complex crack patterning can be reproduced. Therein a limited number of parameters is needed. By applying an elastic-purely brittle local fracture law at the particle level, global softening behavior is observed. The fracture process is realistically described, in particular, when the mode I failure prevails. The disadvantages of this model are the following: the results depend on the beam size and direction of loading, the response of the material is too brittle (due to the assumed brittleness of single beams), the compressed beam elements overlap each other and a big computational effort on the structure level is needed. The first disadvantage can be removed by assuming a heterogeneous structure [39]. In turn, the second drawback can be improved by 3D calculations and consideration of very small particles [28] which increase the amount of crack face bridging and the dissipated energy, and by applying a non-local approach in calculations of beam deformations [39]. In turn, the computational effort was significantly reduced

MOST WIEDZY Downloaded from mostwiedzy.pl

by using a special version of a conjugate gradient solver [39]. In this algorithm, breaking an element and thus removing it from the lattice was a local effect, and the solution required only a few iterations. To improve the lattice behavior in a compression regime, aggregate interlock needs to be considered.

In the second type model (called particle model) [14, 43], the lattice struts connecting adjacent particles transmit axial and shear forces. The struts are not removed. The shear response of struts exhibits friction and cohesion, and the tensile and shear behavior are sensitive to the confining pressure. Due to that the model is suitable for the failure mode I and II. The disadvantage of the model is the fact that it uses a complex macroscopic nonlinear stress-strain relationship to describe a microscopic local behavior.

In our 2D-lattice model, the quasi-brittle material was discretized in the form of a triangular grid including beam elements (as in the lattice model by [39, 28]). The distribution of elements was assumed to be completely random analogously to a Voronoi's construction scheme. First, a triangular grid was created in the material with the side dimensions equal to g (Fig. 2). In each triangle of the grid, additional interior squares were assumed with an area of $s \times s$. Next, one point was selected at random within these interior squares. Later, all points inside the squares were connected with the neighboring ones within a distance of $r_{\max}$ to create a non-uniform mesh of elements, where the maximum element length was $r_{\max}$ (e.g. $r_{\max} = 2g$), the minimum element length was $r_{\min}$ (e.g. $r_{\min} = 0.1g$ for $s = 0.6g$) and the minimum angle between elements was assumed to be α (e.g. $\alpha = 20°$). A uniform triangular mesh could be obtained with parameter

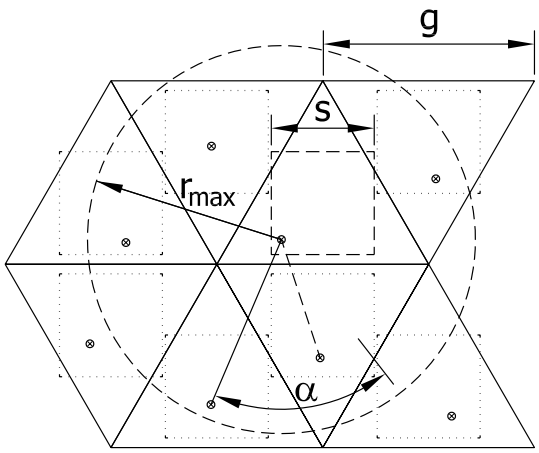

FIG. 2. Scheme to assume a non-uniform distribution of beams in the lattice (s – size of interior squares, $r_{\max}$ – maximum beam radius, a – minimum angle between two beams, g – size of triangular grid)

MOST WIEDZY Downloaded from mostwiedzy.pl

$s = 0$. Using this grid generation method, the elements could cross each other in two-dimensional calculations (similarly as in [11]) but they did not intersect each other in three-dimensional analysis. The elements possessed a longitudinal stiffness described by the parameter k_l (which controls the changes of the element length) and a bending stiffness described by the parameter k_b (which controls the changes of the angle between elements).

In contrast to the lattice method by [39], the model was of a kinematic type, i.e. the calculations of beam displacements were carried out on the basis of consideration of successive geometry changes of elements (which did not posses explicitly any cross-sectional area) due to translation, rotation and deformation (normal and bending). Thus, the global stiffness matrix was not built and the calculation method had a purely explicit character. The displacement of the center of each beam was calculated as the average displacement of two end nodes belonging to the element from the previous iteration step:

$$\Delta\mathbf{X}_i = \frac{\Delta\mathbf{X}_i^A + \Delta\mathbf{X}_i^B}{2}, \tag{2.1}$$

wherein $\Delta\mathbf{X}_i^A$ and $\Delta\mathbf{X}_i^B$ – displacements of the end nodes A and B in the element i, respectively. The displacement vector of each element node was calculated by averaging the displacements of the ends of elements belonging to this node caused by translation, rotation, normal and bending deformations (Fig. 3):

$$\Delta\mathbf{X}^j = \frac{1}{n}\sum_i \left(\mathbf{W}_i^j + \mathbf{R}_i^j\right) + \frac{\sum_i \frac{1}{d_{0_i}}\left(k_{l_i}^j \mathbf{D}_i^j + k_{b_i}^j \mathbf{B}_i^j\right)}{\sum_i \frac{1}{d_{0_i}}\left(k_{l_i}^j + k_{b_i}^j\right)}, \tag{2.2}$$

wherein:

- $\Delta\mathbf{X}^j$ – resultant node displacements,
- $\mathbf{W}$ – node displacement due to the element translation,
- $\mathbf{R}$ – node displacement due to the element rotation,
- k_l – longitudinal stiffness,
- k_b – bending stiffness,
- $\mathbf{D}$ – node displacement due to a change of the element length (induced by the longitudinal stiffness parameter k_l),
- $\mathbf{B}$ – node displacement due to a change of the rotation angle between elements, (induced by the bending stiffness parameter k_b),
- d_{0_i} – initial element length,
- i – successive element number connected with the node j,
- j – node number
- n – number of elements belonging to the node j.

MOST WIEDZY Downloaded from mostwiedzy.pl

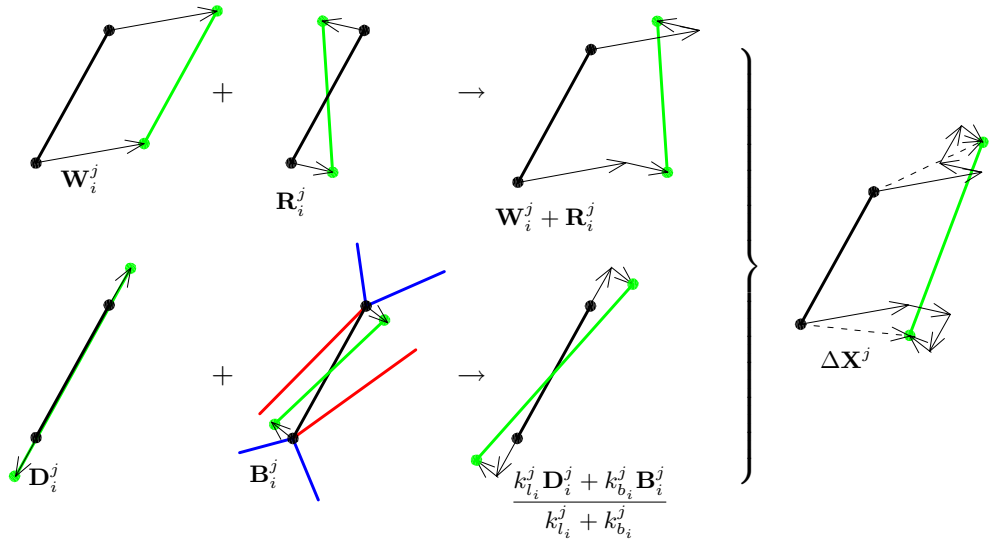

FIG. 3. General scheme to calculate displacements of elements in the lattice.

The node displacements were calculated successively during each calculation step, beginning first from the beam elements subject to prescribed displacements. Next, the resultant force F in a selected specimen's cross-sectional area A is determined (with the aid of the corresponding normal strains ε, shear strains γ, stiffness parameters k_l and k_b, modulus of elasticity E and shear modulus G):

$$F = A \sum \left(\varepsilon k_l E + \gamma k_b G \right), \tag{2.3}$$

where the sum is extended over all elements that cross a selected specimen's cross-section.

For the bending stiffness parameter $k_b = 0$ in Eq. (2.2), the elements behave as simple bars. An element is removed from the lattice if the local critical tensile strain $\varepsilon_{\min}$ was exceeded. All presented numerical calculations were strain-controlled. To perform them, the self-written program was used.

3. Numerical results (one-phase material)

The 2D calculations with a simplified one-phase brittle material were carried out with the specimen of the size 100×100 mm^2 ($b \times h$), composed of 20000 elements distributed non-uniformly ($\alpha = 20^\circ$, $s = 0.6g$, $g \approx 1.5$ mm, $r_{\max} = 2g$). The minimum element length was about 0.6 mm and the maximum one was about 3 mm. The modulus of elasticity of all elements was assumed to be $E = 20$ GPa. The following strain increments were assumed on the basis

MOST WIEDZY Downloaded from mostwiedzy.pl

of initial calculations: 0.000032% (uniaxial compression) and 0.000004% (uniaxial tension). Smaller strain increments only insignificantly influenced the results. The computation time with 20000 elements was about 10 hours using PC 3.6 GHz.

Our lattice model allows us to describe the different Poisson's ratio ν as a function of the parameter stiffness ratio $p = k_b/k_l$. Figure 4 presents the change of the Poisson's ratio ν versus $p = k_b/k_l$ during uniaxial tension, with smooth horizontal edges at the beginning of the deformation process (the elements were not removed). If the stiffness parameter $p = 0.1$, the Poisson's ratio was 0.3. In turn, if the parameter $p > 1$, Poisson's ratio became negative (with the smallest value approximately equal to $\nu = -1.0$ at $p = 10000$). The behavior of elements with values of $p = k_b/k_l$ approaching zero corresponded obviously to that of bars [25, 26, 27].

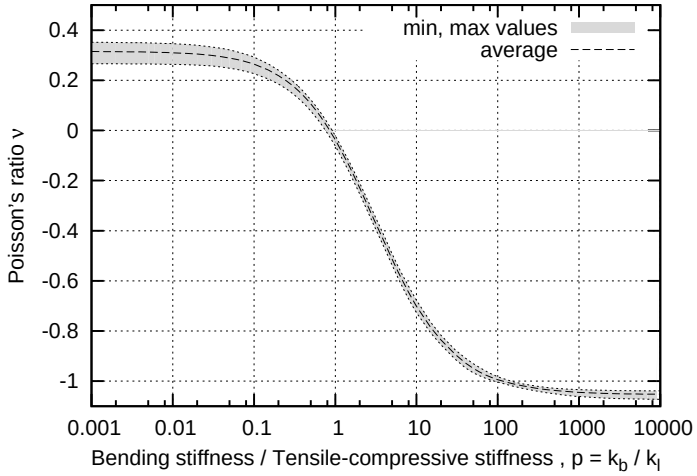

FIG. 4. Influence of the ratio between the bending and longitudinal stiffness $p = k_b/k_l$ on Poisson's ratio ν during uniaxial compression with smooth edges (using semi-logarithmic scale).

The effect of the stiffness parameter $p = k_b/k_l$ on the evolution of the global stress-strain curve σ–ε (vertical normal stress versus the vertical strain) and crack propagation in a specimen during uniaxial compression with smooth edges, is shown in Figs. 5–6 for $\varepsilon_{\min} = 0.02\%$ ($\sigma = P/b$, $\varepsilon = u_2/h$, P – global vertical force, u_2 – vertical displacement of the top edge).

The strength and ductility (ratio between the energy consumed during the fracture process after and before the peak) increase with increasing stiffness parameter p. The material becomes elastic for $p > 0.6$, quasi-brittle for $0.025 > p > 0.01$ and brittle for $p = 0.001$ ($\varepsilon = 0.3\%$). In the last case, the vertical global

MOST WIEDZY Downloaded from mostwiedzy.pl

strain corresponding to the material strength is about 0.03%. The cracks are predominantly vertical (parallel to the loading direction) if $p > 0.2$ (Fig. 6a). In the case of $p < 0.1$, the predominant cracks are more inclined (Figs. 6b and 6c).

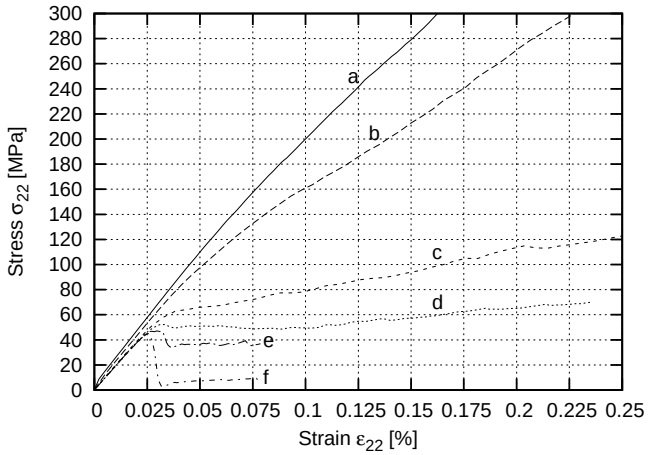

FIG. 5. Effect of the stiffness ratio $p = k_b/k_l$ between the bending stiffness and longitudinal stiffness on the stress-strain curve during uniaxial compression with smooth edges (elements were removed when local $\varepsilon_{\min} = 0.02\%$): a) $p = 0.6$, b) $p = 0.3$, c) $p = 0.06$, d) $p = 0.025$, e) $p = 0.01$, f) $p = 0.001$ (σ_{22} – vertical normal stress, ε_{22} – vertical normal strain).

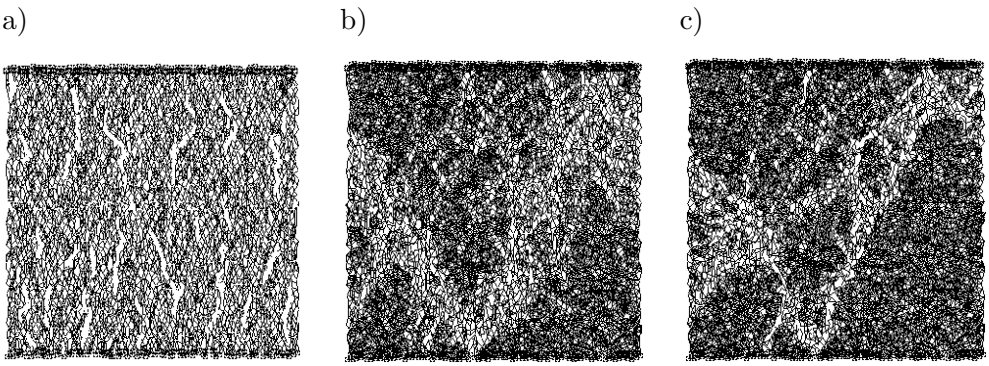

FIG. 6. Effect of the stiffness ratio $p = k_b/k_l$ between the bending and longitudinal stiffness on the crack pattern during uniaxial compression with smooth edges (elements were removed when local $\varepsilon_{\min} = 0.02\%$): a) $p = 0.3$, b) $p = 0.01$, c) $p = 0.001$.

The results for uniaxial tension in a specimen with with a small notch at mid-height of the left side and smooth horizontal edges are demonstrated in Figs. 7, 9a, 10 for the case of $\varepsilon_{\min} = 0.02\%$. The material behaves in the elastic-purely brittle way (Fig. 9a). The strength increases with increasing p, and the brittleness increases with decreasing p (Fig. 7). The overall vertical strain corresponding to the peak stress values is about $0.005 - 0.007\%$ (thus it is smaller

MOST WIEDZY Downloaded from mostwiedzy.pl

than the local $\varepsilon_{\min}$). The crack pattern practically does not depend on the parameter p (Figs. 9a, 10). The main crack is always initiated at the notch and then propagates almost horizontally through the specimen.

The ratio of flexural to axial stiffness p has an inverse effect during compressive fracture as the bending factor α used in a conventional lattice model [28, 39, 44, 48]. The compressive behavior changes namely from brittle to ductile when p increases (α decreases). During tensile fracture, the factor p slightly affects the material behavior. However, the effect of α is negligible.

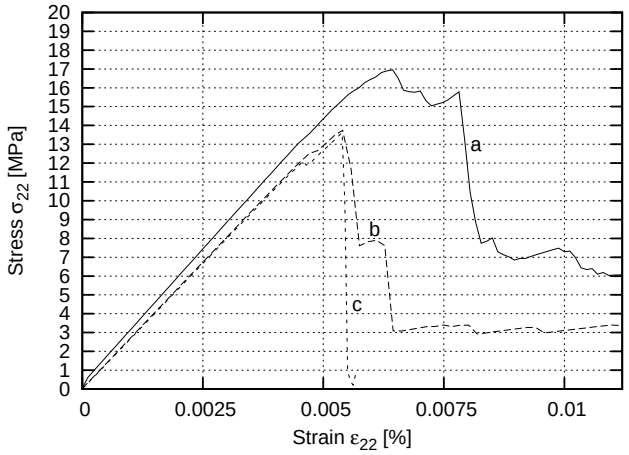

FIG. 7. Effect of the ratio stiffness $p = k_l/k_b$ on the stress-strain curve during uniaxial extension (elements were removed when local $\varepsilon_{\min} = 0.02\%$): a) $p = 0.3$, b) $p = 0.025$, c) $p = 0.001$ (σ_{22} – vertical normal stress, ε_{22} – vertical normal strain).

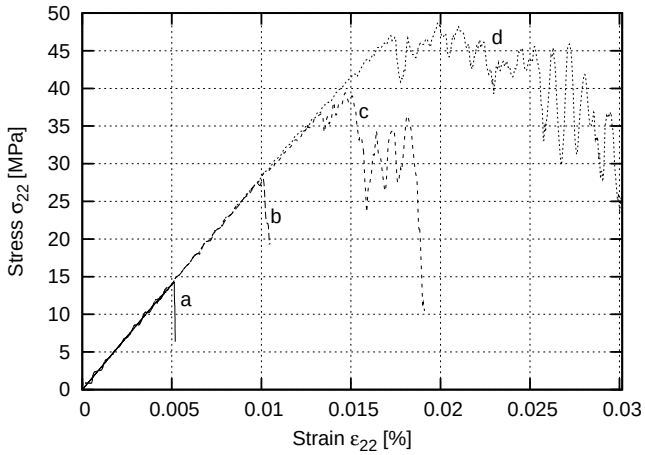

FIG. 8. Effect of the characteristic length on the stress-strain curve ($p = 0.6$, specimen 100×100 mm^2): a) $l_c = 0$ (local approach), b) $l_c = g$, c) $l_c = 2g$, d) $l_c = 3g$ (non-local approach, σ_{22} – vertical normal stress, ε_{22} – vertical normal strain).

MOST WIEDZY Downloaded from mostwiedzy.pl

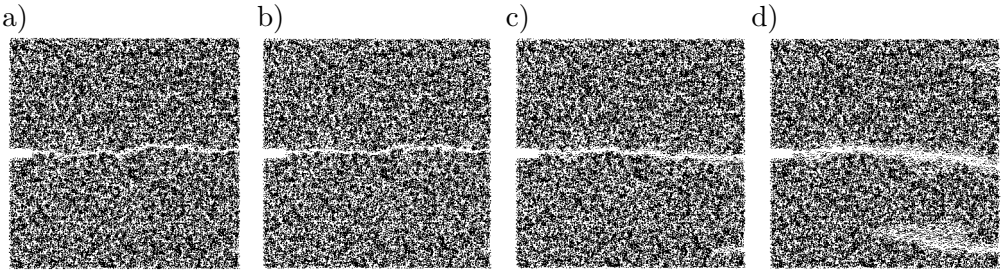

FIG. 9. Effect of the characteristic length l_c on the fracture process (elements were removed when local $\varepsilon_{\min} = 0.02\%$, $p = 0.6$): a) $l_c = 0$ (local approach), b) $l_c = g$, c) $l_c = 2g$, d) $l_c = 3g$ (non-local approach).

To decrease the material brittleness in calculations (which is too large [46] in 2D one-phase material), a non-local approach [5] can be used to calculate strains [27]. In the calculations, the normal strain in each element was assumed to be non-local:

$$\bar{\varepsilon}_k = \frac{\sum w(r)\varepsilon(x_k + r) l \cos(\alpha)}{\sum w(r) l \cos(\alpha)}, \tag{3.1}$$

where x_k – global coordinates of the element, w – weighting function, r – distance between the mid-point of the element and the mid-points of other neighboring elements, l – element length and α – angle between the elements. In general, it is required that the weighting function should not alter the uniform field which means that it must satisfy the normalizing condition [5]. Therefore, as a weighting function $w(r)$ in Eq. 3.1, a Gauss distribution function for 2D problems was used:

$$w(r) = \frac{1}{l_c\sqrt{\pi}} e^{-(r/l_c)^2}, \tag{3.2}$$

where the parameter l_c is a characteristic length of micro-structure. The averaging in Eq. 3.1 is restricted to a small representative area around each material point (the influence of points at the distance of $r = 3l_c$ is only of 0.1%). Figures 8–9 demonstrate the results for a non-local approach during uniaxial tension. In the calculations, the different values of l_c ($l_c = 0, 1 \times g, 2 \times g$ and $3 \times g$) were used. The results show that the strength, normal strain corresponding to the peak and material ductility increase with increasing l_c.

4. Numerical results (two-phase material)

Figures 10–11 show the effect of aggregates on the fracture behavior of 2D specimens under uniaxial extension (without interfacial transition zones).

MOST WIEDZY Downloaded from mostwiedzy.pl

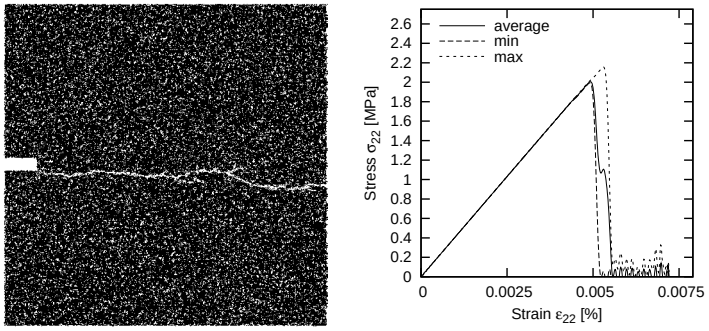

FIG. 10. 2D specimen subject to uniaxial extension (one-phase material): $p = k_b/k_l = 0.7$ (with $k_l = 0.1$) and local $\varepsilon_{\min} = 0.02\%$.

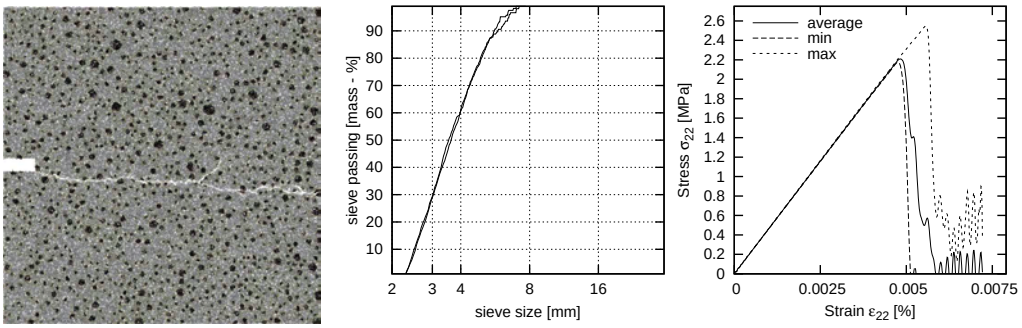

FIG. 11. 2D specimen subject to uniaxial extension (two-phase material): cement matrix: $p_m = k_b/k_l = 0.7$ (with $k_l = 0.1$), local $\varepsilon_{\min} = 0.02\%$ and aggregate: $p_a = k_b/k_l = 0.7$ (with $k_l = 0.3$), local $\varepsilon_{\min} = 0.0133\%$.

The 2D calculations were carried out with a specimen size of 200×200 mm^2 ($b \times h$) composed of 180000 elements distributed non-uniformly ($\alpha = 20°$, $s = 0.6g$, $g = 1$ mm, $r_{\max} = 2g$). The minimum element length was about 0.3 mm and the maximum one was about 2 mm. The moduli of elasticity were: $E = 60$ GPa (aggregate) and $E = 20$ GPa (matrix), respectively [44]. The computation time was about 15 hours using the processor AMD 4600+.

The ratios between the parameters k_l and $\varepsilon_{\min}$ for the cement matrix and aggregate were assumed on the basis of ratios between the elastic Young's moduli and tensile strengths, respectively, assumed in [44]. One choses $p_m = k_b/k_l = 0.7$ (with $k_l = 0.1$) and $\varepsilon_{\min} = 0.02\%$ in the cement matrix, and $p_a = k_b/k_l = 0.7$ (with $k_l = 0.3$) and $\varepsilon_{\min} = 0.0133\%$ in the aggregate. The particle distribution curve for aggregate is shown in Fig. 11 with the mean aggregate diameter of $d_{50} = 3.5$ mm. The aggregate volume density was taken as 50%. This 2D density is smaller than the particle density in real 3D concrete specimen usually equal to 70–75%.

MOST WIEDZY Downloaded from mostwiedzy.pl

The aggregate distribution was generated following the method given in [20]. First, a grading curve was chosen (Fig. 11). Next, certain amounts of particles with defined diameters were generated according to this curve. Finally, the spheres describing aggregates were randomly placed in the specimen preserving the particle density and a certain mutual minimum distance [44]:

$$D > 1.1\frac{D_1 + D_2}{2}, \tag{4.1}$$

where D is the distance between two neighboring particle centers and D_1 and D_2 are the diameters of these two particles.

The results of the uniaxial tensile test in Fig. 11 show evidently that the presence of only the aggregate (without interfacial zone) does not significantly affect the load-displacement curve which remains still too brittle as compared to experiments with concrete specimens [47, 46]. The overall vertical strain ε_{22} corresponding to the peak is about 4 times smaller than the assumed local $\varepsilon_{\min}$ of cement matrix, and 10 times too large as compared to experiments [46].

5. Numerical results (three-phase material)

Figures 12–15 present the results concerning a square concrete specimen considered as a three-phase material. The 2D calculations were carried out mainly with a specimen size of 200×200 mm^2 ($b \times h$) composed of 180000 elements distributed non–uniformly ($\alpha = 20^\circ$, $s = 0.6g$, $g = 1$ mm, $r_{\max} = 2g$). The minimum element length was about 0.3 mm and the maximum one was about 2 mm. The assumed material parameters are given in Table 1. The interface had the lowest strength. The aggregate density was assumed to be 25% or 50%, respectively. The mean aggregate diameter d_{50} was taken as 3.5 mm for the aggregate size of the range $2 - 8$ mm and 12 mm for the aggregate size of the range 2–16 mm. Five simulations were performed for each case. The interfacial zones were added by assigning different properties to the beams which previously connected directly the aggregate with the cement matrix (Fig. 1).

Table 1. Paramaters used in calculation with three-phase material.

Phase	Young's modulus	$p = k_b/k_l$	k_l	local $\varepsilon_{\min}$
Cement matrix	$E_m = 20$ GPa	$p_m = 0.7$	0.010	$\varepsilon_m = 0.2\%$
Aggregate	$E_a = 60$ GPa	$p_a = 0.7$	0.030	$\varepsilon_a = 0.133\%$
Interface bond	$E_b = 14$ GPa	$p_b = 0.7$	0.007	$\varepsilon_b = 0.05\%$

The strength and pre-peak nonlinearity decrease with increasing aggregate density and decreasing mean aggregate diameter. In turn, the material ductility increases when the density increases. The vertical strain corresponding to

MOST WIEDZY Downloaded from mostwiedzy.pl

the peak increases with decreasing particle density. At the low particle content, de-bonding occurs extensively near the isolated aggregates (most of the fractured elements are in bonds). This micro-cracking is responsible for the nonlinear behavior in the pre-peak part of the stress-strain diagram. Next, after the peak, the fracture process progressively spreads through the entire specimen in the form of a macro-crack linking the de-bonded aggregates in lines. With increasing number of aggregates, the fraction of bond elements increases and debonding prevails. At the high particle density, percolation of bond zones occurs, and the condition for macro-crack nucleation and growth occurs early in the loading history. The material becomes significantly weaker (since the interface strength is the weakest component of the system) and the pre-peak nonlinearity does not appear. Since the amount of aggregates is large, the cracks cannot propagate in long lines. Instead of this, several discontinuous macro-cracks propagate in a tortuous manner. The cracks overlap and form branches. As a result, the material ductility grows after the peak. All curves with consideration of interfacial transition zones resemble qualitatively the experimental curves for

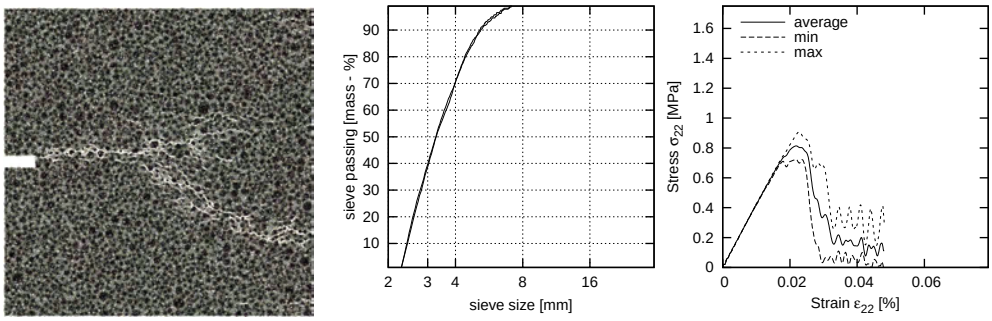

FIG. 12. 2D concrete specimen subject to uniaxial extension (three-phase material), aggregate area percentage 50%, $d_{50} = 3.5$ mm, material parameters as in Table 1 (σ_{22} – vertical normal stress, ε_{22} – vertical normal strain).

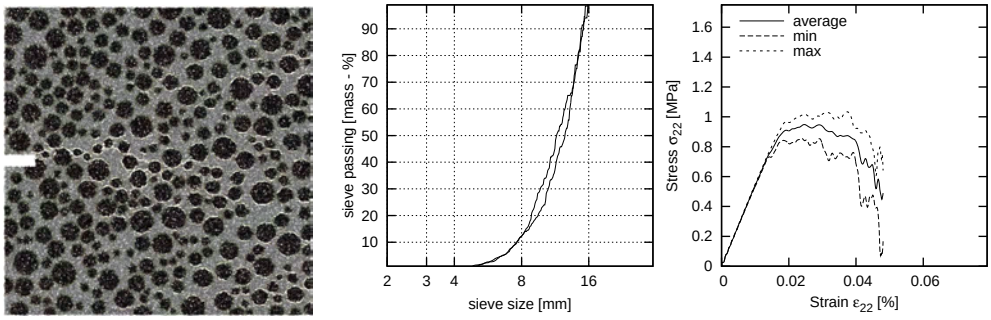

FIG. 13. 2D concrete specimen subject to uniaxial extension (three-phase material) aggregate area percentage 50%, $d_{50} = 12$ mm, material parameters as in Table 1.

MOST WIEDZY Downloaded from mostwiedzy.pl

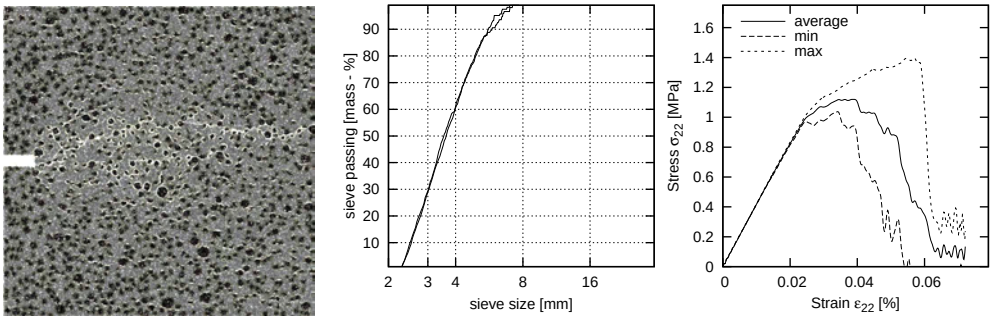

FIG. 14. 2D concrete specimen subject to uniaxial extension (three-phase material) aggregate area percentage 25%, $d_{50} = 3.5$ mm, material parameters as in Table 1.

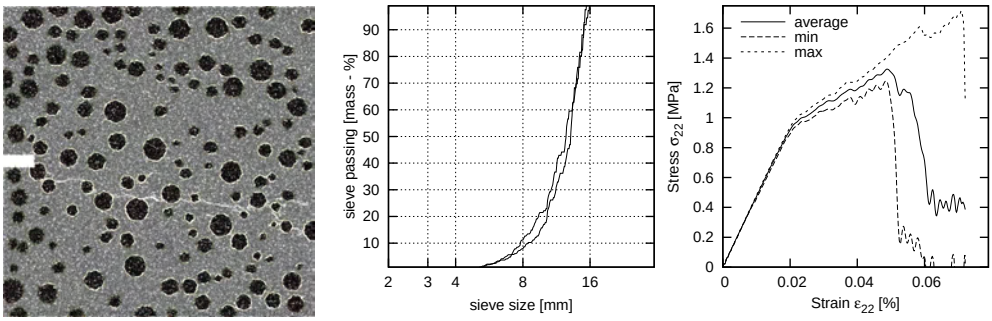

FIG. 15. 2D concrete specimen subject to uniaxial extension (three-phase material) aggregate area percentage 25%, $d_{50} = 12$ mm, material parameters as in Table 1

real concrete [46]. The uniaxial tensile strength changes between 0.7–1.7 MPa. The scatter of the material strength increases with decreasing particle density due to the larger possibility at the choice of the propagation way. The vertical strain ε_{22} corresponding to the peak varies between 0.02–0.06%.

Finally, Figures 16–18 show a deterministic size effect during uniaxial tension (with the grading curve of Fig. 12). Several numerical simulations were carrried out with two different rectangular concrete specimens: 10×10 cm^2 and 20×20 cm^2, using the same beam distribution. The results show that the material strength and ductility increase with decreasing specimen size (as in the experiments (Fig. 17)) while the crack pattern remains similar (Fig. 18). In turn, the fracture energy decreases.

The obtained results of numerical experiments for uniaxial tension are qualitatively in agreement with numerical solutions given in [28, 46, 45].

MOST WIEDZY Downloaded from mostwiedzy.pl

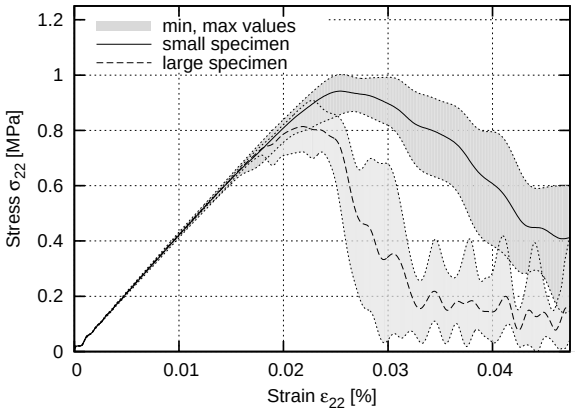

FIG. 16. Deterministic size effect for 2D concrete specimens subject to uniaxial extension with sizes 10×10 cm^2 and 20×20 cm^2, aggregate area percentage 50%, $d_{50} = 3.5$ mm, material parameters as in Table 1.

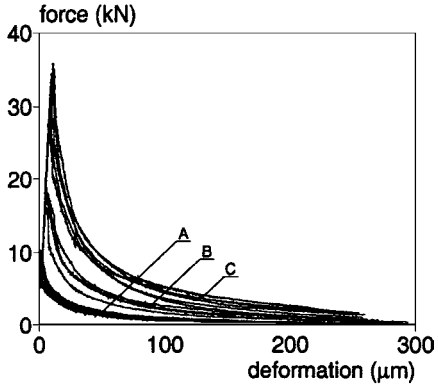

FIG. 17. Experimental force-deformation diagram for 3 different dog-bone shaped specimens $h \times b$: A) 75×50 mm^2 , B) 150×75 mm^2, C) 300×200 mm^2 [46] (h – height, b – width).

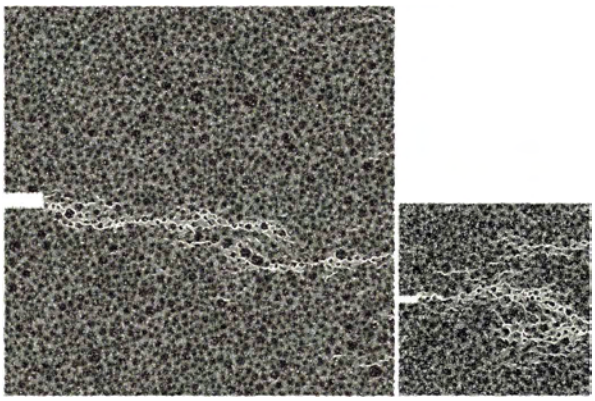

FIG. 18. Fracture in 2 concrete specimens of different sizes (20×20 cm^2 and 10×10 cm^2).

MOST WIEDZY Downloaded from mostwiedzy.pl

6. Conclusion

The lattice model is a simple approach to the fracture behavior in heterogeneous quasi-brittle materials. It is very useful in studying and understanding the phenomenon of the crack formation and crack propagation during uniaxial tension, since it can reproduce fracture processes observed in real laboratory experiments. Owing to this, novel (stronger and better) engineering materials can be developed. By using an elastic-purely brittle local fracture law at the particle level of the material, global softening behavior is obtained. The heterogeneous 2D-lattice model for concrete used in the paper requires 4 material parameters ($k_l, k_b, E, \varepsilon_{\min}$) for each phase and 4 grid parameters (g, s, α and $r_{\max}$) related to the distribution, quantity and length of beam elements. The obtained results of crack patterns and stress-strain curves for a three-phase concrete material during uniaxial tension are qualitatively in agreement with the experimental ones for concrete, and compare quite well with the results published in [46, 28, 45].

The material composition has a significant effect on the material behavior, in particular the particle density and distribution of weak bond zones. The strength and pre-peak nonlinearity decrease with increasing aggregate density and decreasing mean aggregate diameter during uniaxial tension. The material ductility increases when the aggregate density increases. The vertical strain corresponding to the peak increases with decreasing particle density. At the low particle content debonding occurs extensively near the isolated aggregates. At the high particle density, percolation of bond zones occurs, and the condition for macro-crack nucleation and growth appears. The pre-peak nonlinearity cannot be ignored at low particle density. The macro-crack process occurs before the maximum load.

The simulations of a deterministic size effect show a decrease of nominal strength with increasing specimen size as well as an increase of fracture energy with size.

The brittleness in one-phase material can be decreased by using a non-local approach when calculating the strain.

If no bond phase is included, the material strength and material ductility do not depend on the particle density.

The calculations with a lattice model will be continued. First, the model will be extended to 3D. Due to the fact that a realistic aggregate distribution is an essential factor in simulations, the material heterogeneity will be assumed on the basis of digital images of a real concrete specimen. The material parameters for three different phases (k_l, k_b and $\varepsilon_{\min}$) will be identified, on the basis of comparisons of numerical simulations, with different experiments involving strain localization in concrete elements (e.g. bending of notched beams). Sec-

MOST WIEDZY Downloaded from mostwiedzy.pl

ond, a multiscale model will be used linking the lattice model with the continuum elasto-plastic model with non-local softening [8, 10], wherein the first model will be only restricted to the damaged part of the structure.

References

1. P. N. ASFERG, P. N. POULSEN, and L. O. NIELSEN, *Modelling of crack propagation in concrete applying the xfem*, Computational Modelling of Concrete Structures, EURO-C, G. MESCHKE, R. DE BORST, H. MANG and N. BICANIC [Eds.], Taylor anf Francis, 33–42, 2006.
2. Z. P. BAZANT, *Mechanics of distributed cracking*, Appl. Mech. Rev., **26**, 675–705, 1986.
3. Z. P. BAZANT *Scaling of structural strength*, Hermes-Penton, London 2003.
4. Z. P. BAZANT and P. D. BHAT, *Endochronic theory of inelasticity and failure of concrete*, ASCE Journal of Engineering Mechanics, **102**, 701–722, 1976.
5. Z. P. BAZANT and M. JIRASEK, *Nonlocal integral formulations of plasticity and damage: survey of progress*, J. Engng. Mech., **128**, 11, 1119–1149, 2002.
6. Z. P. BAZANT and J. OZBOLT, *Non-local microplane model for fracture, damage and size effect in structures*, ASCE Journal of Engineering Mechanics, **116**, 2485–2505, 1990.
7. Z. P. BAZANT and C. L. SHIEH, *Endochronic model for nonlinear triaxial behaviour of concrete*, Nucl. Engng. Des, 47, 305–315, 1978.
8. J. BOBINSKI and J. TEJCHMAN, *Numerical simulations of localization of deformation in quasi-brittle materials within non-local softening plasticity*, Computers and Concrete, **4**, 433–455, 2004.
9. J. BOBINSKI and J. TEJCHMAN, *Modelling of concrete behaviour with a non-local continuum damage approach*, Archives of Hydro-Engineering and Environmental Mechanics, **52**,2, 85–102, 2005.
10. J. BOBINSKI and J. TEJCHMAN, *Modelling of size effects in concrete using elasto-plasticity with non-local softening*, Archives of Civil Engineering, **52**, 1, 7–35, 2006.
11. N. J. BURT and J. W. DOUGILL, *Progressive failure in a model heterogeneous medium*, ASCE Journal of Engineering Mechanics, **103**, 365–376, 1977.
12. A. CABALLERO, I. CAROL, and C. M. LOPEZ, *New results in 3d meso-mechanical analysis of concrete specimens using interface elements*, Computational Modelling of Concrete Structures, EURO-C G. MESCHKE, R. DE BORST, H. MANG and N. BICANIC [Eds.], Taylor anf Francis, 43–52, 2006.
13. J. CHEN, H. YUAN, and D. KALKHOF, *A nonlocal damage model for elastoplastic materials based on gradient plasticity theory*, Report Nr. 01-13, Paul Scherrer Institut, **1**, 13, 1–130, 2001.
14. G. CUSATIS, Z. P. BAZANT, and L. CEDOLIN, *Confinement-shear lattice model for concrete damage in tension and compression: I. theory*, ASCE Journal of Engineering Mechanics, **129**, 12, 1439–1448, 2003.

MOST WIEDZY Downloaded from mostwiedzy.pl

15. G. A. D'ADDETTA, F. KUN, and E. RAMM *In the application of a discrete model to the fracture process of cohesive granular materials*, Granular Matter, **4**, 77–90, 2002.

16. R. DE BORST, J. PAMIN, and M. GEERS, *On coupled gradient-dependent plasticity and damage theories with a view to localization analysis*, European Journal of Mechanics A/Solids, **18**, 6, 939–962, 1999.

17. M. DI PRISCO and J. MAZARS, *Crush-crack – a non-local damage model for concrete* Mechanics of Cohesive-Frictional Materials, 321–347, 1996.

18. F. V. DONZE, S. A. MAGNIER, L. DAUDEVILLE, and C. MARIOTTI, *Numerical study of compressive behaviour of concrete at high strain rates*, Journal for Engineering Mechanics, 1154–1163, 1999.

19. A. DRAGON and Z. MRÓZ, *A continuum model for plastic-brittle behaviour of rock and concrete*, Int. Journ. Eng. Science, **17**, 121–137, 1979.

20. S. ECKARDT and C. KÖNKE, *Simulation of damage in concrete structures using multiscale models*, Computational Modelling of Concrete Structures, EURO-C G. MESCHKE, R. DE BORST, H. MANG and N. BICANIC [Eds.], Taylor and Francis, 77–83, 2006.

21. H. J. HERRMANN, A. HANSEN, and S. ROUX, *Fracture of disordered elastic lattices in two dimensions*, Physical Rev. B, 39, 637–647, 1989.

22. A. IBRAHIMBEGOVIC, D. MARKOVIC, and F. GATUING, *Constitutive model of coupled damage-plasticity and its finite element implementatation*, Eur. J. Finite Elem., **12**, 4, 381–405, 2003.

23. M. KLISINSKI and Z. MRÓZ, *Description of anelastic deformations and damage for concrete* [in Polish], Technical University of Poznań, 193, 1988.

24. T. A. KOMPFNER, *Ein finites Elementmodell für die geometrisch und physikalisch nichtlineare Berechnung von Stahlbetonschalen* [in Polish], PhD thesis 1983.

25. J. KOZICKI and J. TEJCHMAN, *Discrete methods to describe the behaviour of quasi-brittle and granular materials*, Electronic Proceedings of 16-th Engineering Mechanics Conference ASCE, University of Washington, Seattle, USA, 16.07–18.07.2003, 1–10, 2003.

26. J. KOZICKI and J. TEJCHMAN, *2d lattice model for fracture in brittle materials*, Archives of Hydro-Engineering and Environmental Mechanics, **53**, 2, 71–88, 2006.

27. J. KOZICKI and J. TEJCHMAN, *Modelling of fracture process in brittle materials using a lattice model*, Computational Modelling of Concrete Structures, EURO-C G. MESCHKE, R. DE BORST, H. MANG and N. BICANIC [Eds.], Taylor anf Francis, 139–145, 2006.

28. G. LILLIU and J. G. M. VAN MIER, *3d lattice type fracture model for concrete*, Engineering Fracture Mechanics, **70**, 927–941, 2003.

29. T. C. Y. LIU, A. H. NILSON, and F. O. SLATE, *Biaxial stress-strain relationships for concrete*, ASCE Journal of Engineering Mechanics, **103**, 423–439, 1996.

30. P. MENETREY and K. J. WILLAM, *Triaxial failure criterion for concrete and its generalization*, ACI Structural Journal, 311–318, 1995.

31. Z. MRÓZ, *Mathematical models of inelastic concrete behaviour*, University Waterlo Press, 47–72, 1972.

MOST WIEDZY Downloaded from mostwiedzy.pl

32. H. MÜHLHAUS and E. C. AIFANTIS, *A variational principle for gradient plasticity*, Int. J. Solids Structures, 28, 845–858, 1991.

33. R. PALANISWAMY and S. P. SHAH, *Fracture and stress-strain relationship of concrete under triaxial compression*, ASCE Journal of Engineering Mechanics, 100, 901–916, 1974.

34. J. PAMIN, *Gradient-enhanced continuum models: formulation, discretization and applications, habilitation monograph*, Cracow University of Technology, 2004.

35. J. PAMIN and R. DE BORST, *Simulation of crack spacing using a reinforced concrete model with an internal length parameter*, Arch. App. Mech., **68**, 9, 613–625, 1998.

36. R. H. PEERLINGS, R. DE BORST, W. A. M. BREKELMANS, and M. G. D. GEERS, *Gradient-enhanced damage modelling of concrete fracture*, Mechanics of Cohesive-Frictional Materials, 3, 323–342, 1998.

37. S. PIETRUSZCZAK, J. JIANG, and F. A. MIRZA, *An elastoplastic constitutive model for concrete*, Int. J. Solids Structures, **24**, 7, 705–722, 1988.

38. G. PIJAUDIER-CABOT and Z. BAZANT, *Nonlocal damage theory*, ASCE Journal of Engineering Mechanics, **113**, 1512–1533, 1987.

39. E. SCHLANGEN and E. J. GARBOCZI, *Fracture simulations of concrete using lattice models: computational aspects*, Engineering Fracture Mechanics, **57**, 319–332, 1997.

40. A. SIMONE and L. SLUYS, *Continous-discountinous modeling of mode-i and mode-ii failure*, Modelling of Cohesive-Frictional Materials P.A. VERMEER, W. EHLERS, H. J. HERRMANN and E. RAMM [Eds.], Balkema, 323–337, 2004.

41. L. SLUYS, *Wave propagation, localisation and dispersion in softening solids*, PhD thesis. Delft University of Technology, 1992.

42. L. SLUYS AND R. DE BORST, *Dispersive properties of gradient and rate-dependent media*, Mech. Mater., **183**, 131–149, 1994.

43. K. TAJIMA and N. SHIRAI *Numerical prediction of crack width in reinforced concrete beams by particle model*, Computational Modelling of Concrete Structures, EURO-C G. MESCHKE, R. DE BORST, H. MANG and N. BICANIC [Eds.], Taylor anf Francis, 221–230, 2006.

44. J. G. M. VAN MIER, E. SCHLANGEN, and A. VERVUURT *Lattice type fracture models for concrete*, Continuum Models for Materials with Microstructure, H.B. MÜHLHAUS [Ed.], John Wiley & Sons, 341–377, 1995.

45. J. G. M. VAN MIER and M. R. A. VAN VLIET, *Influence of microstructure of concrete on size/scale effects in tensile fracture*, Engineering Fracture Mechanics, **70**, 16, 2281–2306, 2003.

46. M. R. A. VAN VLIET, *Size effect in tensile fracture of concrete and rock*, PhD thesis, 2000.

47. M. R. A. VAN VLIET and J. G. M. VAN MIER, *Experimental investigation of concrete fracture under uniaxial compression*, Mechanics of Cohesive-Frictional Materials, **1**, 115–127, 1996.

48. A. VERVUURT, J. G. M. VAN MIER, and E. SCHLANGEN, *Lattice model for analyzing steel-concrete interactions*, Computer Methods and Advances in Geomechanics, SIRIWARDANE and ZAMAN [Eds.], Balkema, Rotterdam 713–718, 1994.

MOST WIEDZY Downloaded from mostwiedzy.pl

49. R. VIDYA SAGAR, *Size effect in tensile fracture of concrete – a study based on lattice model applied to ct-specimen, cd-rom*, Proc. 21th Intern. Congress on Theoretical and Applied Mechanics, ICTAM04, pp. 1–2, Warsaw 2004.

50. G. WELLS and L. SLUYS, *A new method for modeling of cohesive cracks using finite elements*, Int. Journ. for Numerical Methods in Engineering, **50**, 12, 2667–2682, 2001.

51. H. M. ZBIB and C. E. AIFANTIS, *A gradient-dependent flow theory of plasticity: application to metal and soil instabilities*, Appl. Mech. Reviews, **42**, 11, 295–304, 1989.

Received November 6, 2006; revised version May 30, 2007.

MOST WIEDZY Downloaded from mostwiedzy.pl